Journal of Physics and Chemistry of Solids 193 (2024) 112177

Contents lists available at ScienceDirect

Journal of Physics and Chemistry of Solids

journal homepage: www.elsevier.com/locate/jpcs

Thermal and spectroscopic (IR, NMR) studies of bulk ammonia borane – Polyethylene oxide composites: A potential hydrogen storage system

Krishna Kharel [a], Riqiang Fu [b], Emily Ingram [a], Caitlyn Clark [a], Özge Günaydın [a,*]

[a] Department of Chemistry and Biochemistry, Lamar University, Beaumont, TX, 77710, USA
[b] The National High Magnetic Field Laboratory, 1800 E. Paul Dirac Drive, Tallahassee, FL, 32310, USA

ARTICLE INFO

Keywords:
Ammonia borane
Polyethylene oxide
MAS-NMR
DSC
ATR/FTIR

ABSTRACT

We utilized differential scanning calorimeter (DSC), Fourier-transformed infrared spectroscopy (FT-IR), and solid-state nuclear magnetic resonance spectroscopy (NMR) techniques to understand the dehydrogenation mechanism of ammonia borane (AB) and its polymer composites. The results indicated that the polymeric composites with higher polyethylene oxide (PEO) mass ratio involve the possible breakdown of dative bond and the formation of new interaction (H-bonding) between the AB and the polymer. The activation energies were calculated in the temperature range of 25 °C and 300 °C which were found to be lower than the pristine AB. ^{15}N and ^{11}B NMR studies at room temperature showed evidence for a possible interaction, H-bonding, between AB and PEO. The NMR experiments at 85 °C were conducted to investigate the isothermal decomposition during several hours. Results indicated that the pristine AB takes longer incubation time, however the polymeric composite readily decomposes at 85 °C. Both showed proof for the formation of byproducts. Moreover, IR study showed evidence to support the interaction between AB and PEO.

1. Introduction

Storing hydrogen, and hydrogen-like light element will revolutionize the electrochemical energy conversion process by making energy supply system more-lighter and efficient. Hydrogen is one of the most attractive alternative energy carrier. It is the ninth most abundant element in the earth crust, (1400 mg/kg), second most abundant element in the ocean, (1.08×10^5 mg/L), high energy to mass ratio (120 kJ/g) which is 3 times higher than the petroleum [1]. Other than that, hydrogen gas when oxidized gives only water as a byproduct.

In chemical storage method to store hydrogen it is produced by the chemical reaction. The most common chemicals used for chemical hydrogen storage are ammonia [2,3], metal hydride [4], formic acid [5], carbohydrates [6], methane [7], methanol [8], liquid organic hydrogen carriers (LOHC) [9] and ammonia borane [10–13].Boranes have been widely studied as a candidate for solid-state hydrogen storage medium [14], and ammonia borane (AB) is one of the promising candidate [15]. AB is a white crystalline powder at room temperature with melting point of 115 °C [16]. Some literature has reported different melting point, 112–114 °C [17–19]. AB has the dipole moment of 5.05 D. The density of AB is 0.74 g/cm^3, and the molecular weight is 30.7 g/mol [17].

The presence of dihydrogen bond (DHB) in AB makes it way different from its isoelectric partner ethane. DHB is the electrostatic interaction between protic and hydridic hydrogen [20]. DHB makes it possible to dehydrogenate at relatively lower temperature below 100 °C [21]. The dehydrogenation of AB was first studied using thermomanometry, pyrolysis, DSC, DTA and TGA [22]. It was found that the thermal decomposition of AB starts at around 120 °C. While decomposing AB to 300 °C a white solid residue was obtained. AB upon pyrolysis released H_2 along with the mixture of polyaminoborane, polyimidoborane, borazine [23]. At melting point, DSC curve showed the sharp endothermic peak at 115 °C [16]. The endothermic peak is followed by exothermic peak considered as first hydrogen release at 117 °C [16]. Although, AB has 3 equivalent hydrogen, it is possible to get only 2 equivalent hydrogen below 300 °C.

Despite having all these benefits, application of AB in real world is limited only in lab because the rate of hydrogen release below 85 °C requires longer incubation time. In addition, during thermolysis AB decomposes to give borasic impurities that may poison the fuel cell, the release of other volatiles like borazine, ammonia during decomposition of ammonia borane, hydrogen get trapped in those compounds and wasted, foaming during hydrogen release is another problem [24,25].

* Corresponding author.
E-mail addresses: gkrishnakharel@gmail.com (K. Kharel), rfu@magnet.fsu.edu (R. Fu), eingram1@lamar.edu (E. Ingram), cclark17@lamar.edu (C. Clark), ozge.sen@lamar.edu (Ö. Günaydın).

https://doi.org/10.1016/j.jpcs.2024.112177
Received 19 December 2023; Received in revised form 7 June 2024; Accepted 27 June 2024
Available online 27 June 2024
0022-3697/© 2024 Elsevier Ltd. All rights are reserved, including those for text and data mining, AI training, and similar technologies.

Moreover, even during hydrolysis of ammonia borane using the catalyst Au@Cu_2O core@shell nanocrystals, ammonia and borate are released which not just wasted the hydrogen in the form of ammonia but also poisoned the catalyst [26].

To decrease the dehydrogenation temperature and improve the kinetic properties of AB, various approaches to modify AB has been studied. The examples include dispersion in polymer matrix like polyacryl amide (PAM) [16,27], poly(methyl acrylate) (PMA) [28], polyethylene oxide (PEO) [18,29], polyvinylpyrrolidone (PVP) [23–32], poly(amidoamine) (PAMAM) [33] nanoconfinement [34–38], ruthenium-based cat.lyst [39,40], palladium based catalyst [41] platinum-based catalyst [42,43], bimetallic catalyst like $Ni_{1-x}Pt_x$ [44], CoNi [45], PdPt nanocubes [46], platinum-loaded titanium dioxide [47], dispersion in organic and ionic liquid [48], nanoconfinement of ammonia borane into metal organic frameworks (MOFs) like Isoreticular metal-organic frameworks (IRMOFs) and UiO-66 [49], platinum nanoparticle functionalized carbon nanotubes [42], AB milled with zeolite ZIF-8, AB milled with nonporous zinc chloride [50]. Use of Tm based MOFs (Tm(BTC)-CH_3OH) not only decreased the dehydrogenation temperature but also eliminated the formation of degradants like ammonia, diborane and borazine [51].

In the current study, we prepared composites of AB with high M_v (400,000) PEO using sol-gel technique with slight modification on the method explained by Li et al. [27] A catalyst, $MgCl_2$,was also added to study the effect of alkaline earth metal on dehydrogenation. We performed, high-temperature dehydrogenation study using standard and isothermal mode of DSC. The decomposed sample were further studied using IR technique. Furthermore, we used room temperature ^{15}N CP-MAS NMR, room temperature and isothermal ^{11}B MAS-NMR to understand the dehydrogenation in ABPEO composites. All the isothermal studies were performed at 85 °C. The enhanced dehydrogenation efficiency observed in ABPEO compared to pristine AB can be attributed to several key mechanistic factors. One significant aspect is the presence of $MgCl_2$ catalyst, which plays a pivotal role in facilitating the dehydrogenation process by promoting hydrogen release through destabilization of the AB bonds resulting in the release of H_2 molecule from the catalyst complex [52]. Additionally, as per the density functional theory calculation, the introduction of PEO chain in AB can result in the increased electron density in the AB molecule due to the interaction of the ethereal oxygen atom with the protic hydrogen atom in the amine moiety of AB molecule. As a result of which the hydridic hydrogen atom become more negatively charged resulting in the greater nucleophilicity of the hydrides which enhance the formation of highly polar diammoniate of diborane (DADB) an intermediate ion which is unstable in PEO Solution leading to rapid oligomerisation accompanied by the release of hydrogen [18].

2. Experimental

2.1. Materials

Ammonia borane (AB, NH_3BH_3 97 % pure), PEO ($M_v = 400{,}000$) and $MgCl_2$ were all purchased from sigma aldrich and used as received.

2.2. Preparation of ABPEO composites

AB (0.1 g) was first dissolved in 1 ml of water. For the preparation of 1:1 ratio of AB and PEO (ABPEO11), the same proportion of PEO was weighed and put into the schlenk flask where 1 ml of aqueous AB was added. We have modified the sol-mixing technique as mentioned by Li et al. [27] to make the transfer easier which did not make any difference in spectroscopic and thermal studies. The amount of water used was 10 wt% to maintain the viscosity so that there will be proper mixing of AB in the PEO matrix. The gel was stirred for 6 h to confirm the uniform mixing and later it was dried under vacuum for six more days to confirm the uniform drying of the sample [16,27,30]. The composites with the mass ratio of 1:2 (ABPEO12) and 1:3 (ABPEO13) was prepared by using 0.05 g and 0.025 g of AB respectively and repeating the same process. Similarly, for the preparation of cat.ABPEO ($MgCl_2$ doped ABPEO composites), $MgCl_2$ (1 g) was dissolved in water, and the final volume was made to 10 ml, and the primary stock solution was prepared. The concentration needed for the experiment was obtained by the serial dilution from the primary stock solution to 10 ml. The mixture was stirred for 6 h then dried under vacuum for six days. By this time, a rubbery material of AB/PEO doped with $MgCl_2$ was obtained and stored in a desiccator until further use. The composites with the mass ratio of 1:2 and 1:3 was prepared by dissolving 0.05 g and 0.025 g of AB in the $MgCl_2$ solution.

2.3. Characterization

Dehydrogenation study of AB and its polymeric composites were performed using Q20 differential scanning calorimeter DSC in standard and isothermal mode. In isothermal mode, pristine AB and bulk composites were heated at 85 °C for 1 h.3–5 mg of sample was loaded in standard aluminum pan with small hole on the lid. The hole serves as an outlet for the hydrogen gas and other volatile components during decomposition. The samples were heated from 25 to 300 °C to investigate dehydrogenation kinetics. Different ramp rates (1, 3, 5, 10, 15 and 20 °C/min) were used to study the linear dependence of dehydrogenation temperature with ramp rate. The linear dependence enables us to determine the activation energy using Ozawa and Kissinger methods as shown in equations I and II below where β is the ramp rate, R is the gas constant, E_a is the activation energy, T is the temperature.

- Ozawa method [53].

$$ln\,\beta = \frac{-E_a}{RT_d} + C \tag{I}$$

- Kissinger method [53,54].

$$ln\left(\frac{\beta}{T_d^2}\right) = \frac{-E_a}{RT_d} + C \tag{II}$$

Nicolet iS50 FTIR/ATR was used to study the different modes of vibration, change in vibration frequency (Δω) in pristine AB and its polymeric composites. The resolution for IR study was 2 cm^{-1} with 64 number of scans. All NMR measurements were carried out on a Bruker Avance 600 MHz (14.1 T magnet) NMR spectrometer with Larmor frequencies of 60.81 and 192.55 MHz for ^{15}N and ^{11}B, respectively, using a Bruker 4 mm double-resonance MAS NMR probe. The sample spinning rate was controlled within 10 kHz ±3 Hz by a Bruker pneumatic MAS control unit. ^{15}N was performed to understand the changes in nitrogen environment in ABPEO composites. The ^{15}N signals were enhanced through cross polarization (CP) from protons with a contact time of 1 ms, during which a 1H spin-lock field of 35 kHz was used and the ^{15}N radiofrequency was ramped from 30 to 40 kHz. During the ^{15}N acquisition, a high power ^{1}H decoupling was used. A range of 1000–7000 scans was used to accumulate the ^{15}N signals with a recycle delay of 15 s. The ^{15}N chemical shifts were referenced to the ammonium nitrogen resonance of glycine at 33.2 ppm. Similarly, ^{11}B MAS-NMR was carried out for the isothermal dehydrogenation study to have an insight on the change in boron environment and to study the of incubation time. The ^{11}B signals were recorded using the standard spin-echo sequence with a 90° pulse length of 2.25 μs and the echo time of 400 μs (4 rotor periods) with a recycle delay of 2 s. AB and its polymeric composites were heated at 85 °C for 6 h during this study.

3. Results and discussion

3.1. Thermal decomposition of AB and its polymeric composites

Thermolytic decomposition of AB and its composites were performed from 25 °C to 300 °C to understand the dehydrogenation properties. The graph between heat flow versus temperature was plotted to track the changes in melting point (T_m) and decomposition temperature (T_d) of AB and its composites as shown in Fig. 1 (a.) and (b.) The melting and decomposition of the sample were noticed with a sharp endothermic and exothermic peak respectively in the thermogram. For pristine AB and PEO, the first endothermic peak referred to as melting was observed at 113 °C and 68 °C respectively. However, upon trapping AB in a polymer matrix, there is a significant reduction in T_m and foaming of AB. The reduced foaming effect, when mixed in polymer matrix, is contributed to the change in dihydrogen bonding network [18]. The first hydrogen release for pristine AB was observed at 118 °C. Upon the addition of polymer in AB, the first hydrogen release at a ramp rate of 5 °C/min for ABPEO11, ABPEO12, ABPEO13 was detected at 108 °C, 107 °C, and 104 °C respectively.

We observed two different peaks below 120 °C after using 5 wt % of $MgCl_2$, the first peak for cat.ABPEO11, cat.ABPEO12, and cat.ABPEO13 at a ramp rate of 5 °C/min was detected at 85 °C, 85 °C, and 94 °C respectively. The second peak for cat.ABPEO11, cat.ABPEO12, and cat. ABPEO13 was observed at 108 °C, 108 °C, and 109 °C respectively.

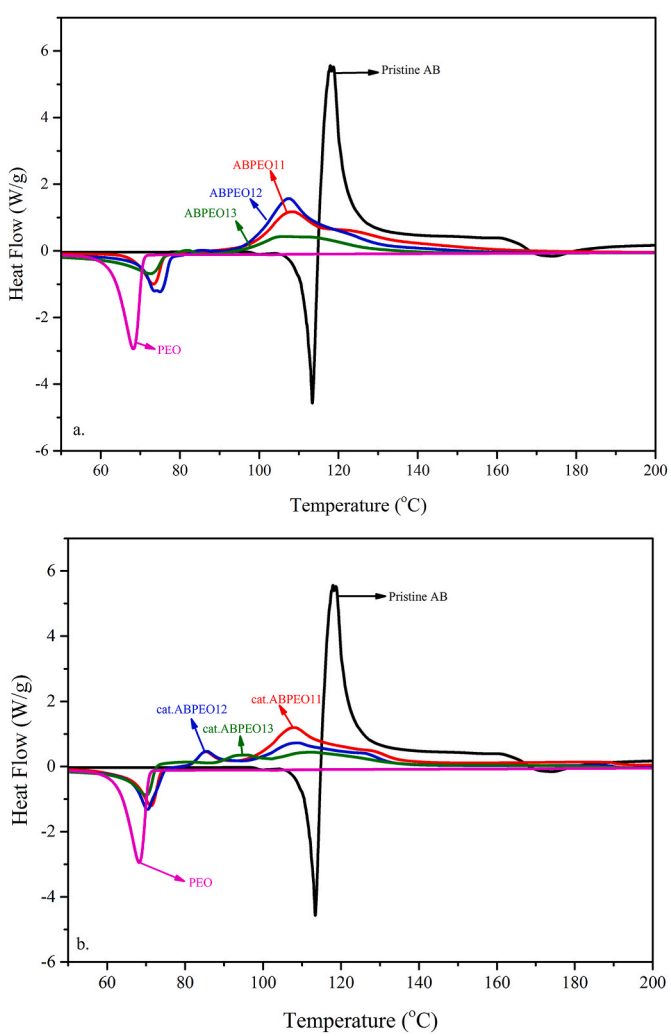

Fig. 1. Decomposition of AB and ABPEO composites without catalyst (a.) and with catalyst (b.) with the ramp rate of 5 K/min.

Fig. 1 (a.) and (b.) shows the melting and hydrogen release of pristine AB and different ABPEO composites with and without the catalyst. No significant difference for different polymeric composites regarding dehydrogenation temperature was observed. However, the most obvious change was the dehydrogenation temperature being lower upon using 5 % $MgCl_2$ when compared with pristine AB. The dehydrogenation temperature started to increase when 75 % PEO was used in the composites. For all the ramps, the dehydrogenation temperature first decreased and later started to increase with the increase in the polymeric content. While comparing the melting point of different polymeric composites, the one with the catalyst was lower than the one without for ABPEO11 and ABPEO12 composites, ABPEO11 = 71.8 °C, and cat.ABPEO11 = 68.7 °C, ABPEO12 = 73.5 °C and cat.ABPEO12 = 70.32 °C. Unlike ABPEO11 and ABPEO12 composites, the melting point for ABPEO13 was almost the same for the one with catalyst and without catalyst ABPEO13 = 67.9 °C and cat.ABPEO13 = 68.0 °C.

3.2. Kinetic studies of AB and ABPEO composites

AB and ABPEO composites were heated from 25 °C to 300 °C with the ramp rates of 1, 3, 5, 10, 15 and 20 °C/min for the kinetic study. The activation energies were determined by Ozawa and Kissinger methods [16,30]. The corresponding increase in the decomposition temperature for the composites are linearly correlated with the ramp rate. This correlation between heating rate and decomposition temperature was utilized to determine the activation energy of pristine AB and different polymeric composites.

Figs. 2 and 3 show the activation energy fits by using Kissinger method. The activation energies for pristine AB were calculated to be 149 and 155 kJ/mol by Kissinger and Ozawa method respectively. Similarly, the activation energy for different polymeric composites of AB with and without catalyst was determined. The activation energies for ABPEO11, ABPEO12, ABPEO13 were calculated to be 115 kJ/mol, 113 kJ/mol, 144 kJ/mol according to Kissinger method and 115 kJ/mol, 119 kJ/mol, and 137 kJ/mol according to Ozawa method. Similarly, the activation energies for the catalytic polymeric composites of AB were determined to be 118 kJ/mol, 114 kJ/mol, and 108 kJ/mol according to Kissinger method and 124 kJ/mol, 120 kJ/mol, 114 kJ/mol according to Ozawa method for cat.ABPEO11, cat.ABPEO12 and cat.ABPEO13 respectively. There is a significant difference in the activation energy of pristine AB and different polymeric composites showing enhanced kinetic. However, when polymeric ratio increases, the E_a value started to increase. The polymeric composites with the catalyst showed earlier

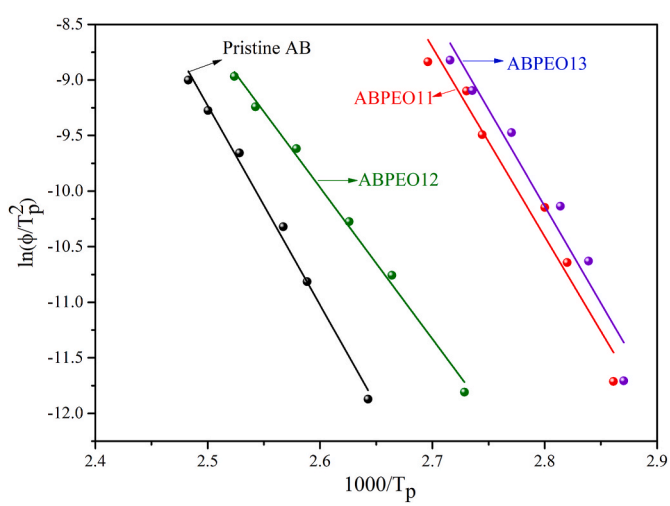

Fig. 2. Activation energy fits by using Kissinger method for AB (black) and ABPEO11 (red), ABPEO12 (blue) and ABPEO13 (green) composites without using catalyst.

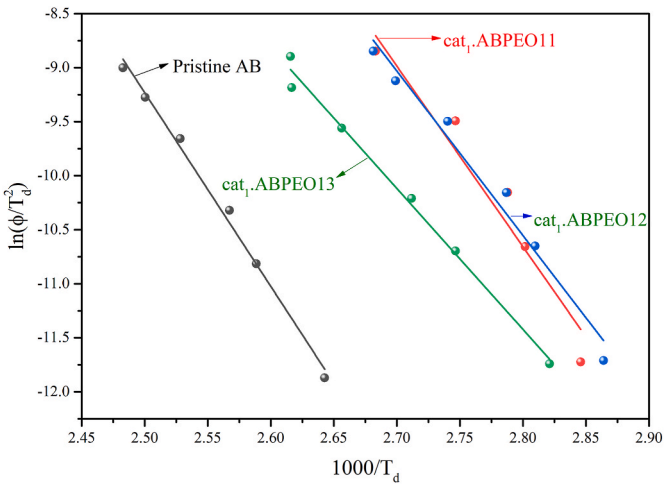

Fig. 3. Activation energy fits for first hydrogen release using Kissinger method for AB (black), Cat$_1$.ABPEO11 (red), Cat$_1$.ABPEO12 (blue) and Cat$_1$.ABPEO13 (green) composites with a catalyst.

decomposition as shown in Fig. 1 (a.) and (b.) However, regarding activation energy, there is no significant improvement. Table 1 displays the activation energy by Ozawa and Kissinger method (Standard deviation is in the range of ±3–5 for all, except 1:3 ratio is about ±10 kJ/mol) and the hydrogen release temperature at ramp 5 °C/min. Unlike other polymers, as reported by Kharel et al. [16] and Seemaladinne et al. [30], the dehydrogenation temperature started to increase with the 75 % polymeric composites with the catalyst. This could be due to the interaction between the formation of new $MgCl_2$/AB phase as explained by Ding et al. [55] and PEO. Additionally, this may also be due to interaction between PEO/$MgCl_2$ system which is the ratio of molar of etherial oxygen atom to the molar of magnesium cation as explained by Yang et al. [56] and AB. Yang et al. explained the formation of two different crystalline phase which corresponds to pure PEO and the $MgCl_2$ complex and coexisting elastomeric phases [57]. Furthermore, having less amount of AB (about 25 %) in cat.ABPEO13 composite, all the AB present might have formed new $MgCl_2$-AB-PEO complex which is entirely different from $MgCl_2$/AB complex and ABPEO complex by itself. And it might have increased the dehydrogenation temperature when compared to the corresponding cat.ABPEO11 and cat.ABPEO12.

Table 1
Activation energy values of AB and its composites with first hydrogen release and melting point.

Sample	AB (%)	PEO (%)	E_a (Ozawa)	E_a (Kissinger)	T_m	T_d
PEO	0	100			68.2	–
AB	100	0	155.6	149.1	113.3	117.9
ABPEO11	50	50	122.2	108.0	73.4	108.3
ABPEO12	33.3	66.6	119.6	113.3	73.6	107.5
ABPEO13	25	75	137.5	131.1	72.5	104.6
Cat$_1$. ABPEO11	50	50	145.6	138.0	71.2	85.3
Cat$_1$. ABPEO12	33.3	66.6	173.5	167.5	70.3	85.5
Cat$_1$. ABPEO13	25	75	114.5	108.4	70.0	94.4
Cat$_2$. ABPEO11	–	–	124.8	118.5	–	94.0
Cat$_2$. ABPEO12	–	–	120.7	113.3	–	93.6
Cat$_2$. ABPEO13	–	–	110.6	104.2	–	97.9

$E_{a(Kissinger)}$ = Activation energy by Kissinger method in kJ/mol, $E_{a(Ozawa)}$ = Activation energy by Ozawa method in kJ/mol, T_m = Melting temperature in °C, T_d = Hydrogen release temperature at ramp 5 °C/min, Cat$_{1.}$ = polymeric composite with catalyst and subscript 1 stands for the first peak (i.e. first hydrogen release), Cat$_2$. = polymeric composite with catalyst and subscript 2 stands for the second peak (i.e. second hydrogen release). The ratio between AB and PEO for the composites with catalyst are same as the one without catalyst. The composites with catalyst were doped with 10 mg of $MgCl_2$ for AB used.

3.3. Spectroscopic studies

3.3.1. IR studies

3.3.1.1. Room temperature IR (ATR) studies of AB and its polymeric composites. To understand the vibrational properties of AB and its composites we performed solid state Fourier Transform Infrared Spectroscopic studies at room temperature for pristine AB and its composites was performed. Vibrational properties of the decomposed sample at 85 °C was also studied. There was no significant difference detected in the IR spectrum with catalyst from without catalyst.

Fig. 4 shows the ATR spectra of pure AB and PEO at room temperature with proper peak assignment. N–H stretching was seen in the region between 3000 and 3500 cm^{-1}. The peaks at around 3317 and 3250 cm^{-1} were assigned for the N–H asymmetric and symmetric stretching mode respectively. The peaks are in proper agreement as reported by Petit et al. [58] and Smith et al. [59] Similarly, the peaks at 3194 and 3172 cm^{-1} were assigned as N–H … …H–^{10}B and N–H … …H–^{11}B hetero-polar interaction. The peaks in the region of 2500 to 2000 cm^{-1} were assigned to the B–H stretching mode. At room temperature, in B–H stretching mode of pristine AB and its composites shows five different peaks. The peaks at 2379 and 2329 cm^{-1} were assigned for the asymmetric stretching of ^{11}B–H and ^{10}B–H stretching mode respectively. Similarly, the peaks at 2280 and 2214 cm^{-1} were assigned for ^{11}B–H and ^{10}B–H symmetric stretching. The small peaks at 2114 and 1895 cm^{-1} are due to the N–H … …H–^{11}B and N–H——H–^{10}B heteropolar interaction. Petit et al. reported the similar kind of interaction [58]. They observed the stretching modes at 2372 cm^{-1} (asymmetric), 2310 cm^{-1} (symmetric) and 2276 cm^{-1} (asymmetric) and 2210 cm^{-1} (symmetric) for ^{10}B–H and ^{11}B–H respectively [58]. According to Xie et al., 2453 cm^{-1}and 2337 cm^{-1} were assigned as BH asymmetric and symmetric modes respectively. However, they did not give any clue regarding the presence of vibration mode for different isotopes of boron [60].

Fig. 5 displays the ATR spectrum of AB and its composites without catalyst at room temperature. The dotted lines in Fig. 5 display the proper alignment of the different vibration modes with AB and different polymeric composites. The difference in the vibration frequency for different polymeric composites in NH_3 deformation region was observed probably due to the interaction caused by PEO. The asymmetric and

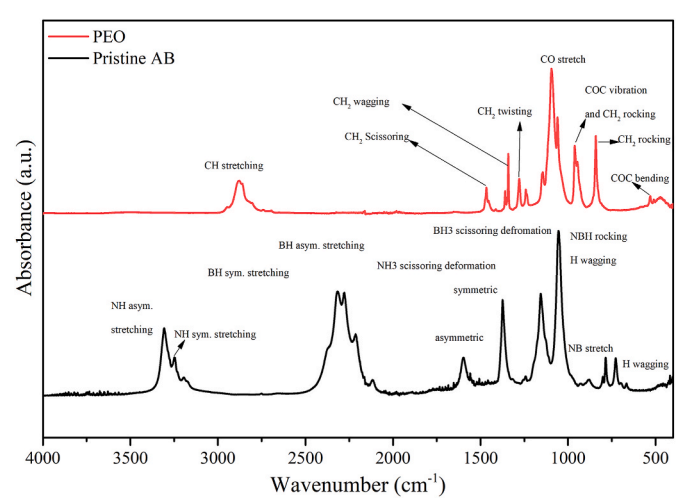

Fig. 4. The ATR spectrum of AB and PEO vibration modes.

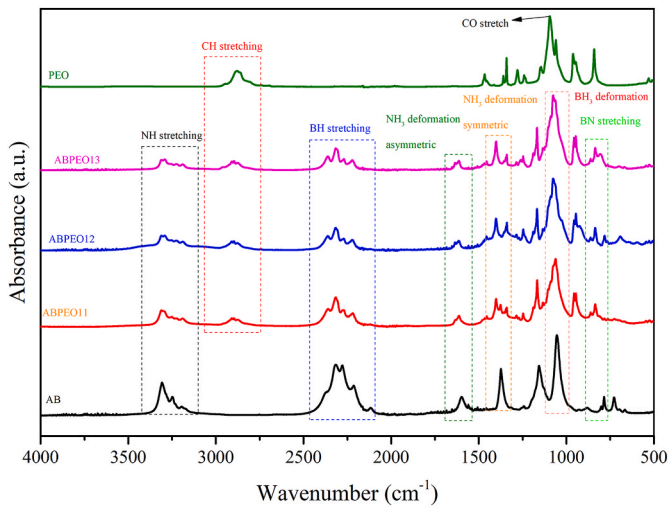

Fig. 5. ATR spectrum of AB and its composites without catalyst.

symmetric NH_3 deformation for pristine AB were detected at 1603 and 1376 cm^{-1} respectively. Different literature observed NH_3 deformation at 1602 [61], 1599 [58], 1584 [60], 1597 [62](asymmetric) and 1375 [61], 1373 [58], 1362 [60], 1372 [62] (symmetric) cm^{-1}. $\Delta\omega$ is the difference in the wavenumber between AB and the composite for specific region of our interest. $\Delta\omega$ is the change in the vibration frequency for different vibration modes relative to pure AB. The higher $\Delta\omega$ indicates the relative change in the interaction probably due to breaking of dihydrogen bonding network present in pristine AB or change in the characteristic of dative bond due to the presence of electron dense ethereal oxygen. NH_3 asymmetric deformation for different polymeric composites, ABPEO11, ABPEO12 and ABPEO13 were observed at 1609 ($\Delta\omega = 6.0$), 1625 ($\Delta\omega = 22.0$) and 1628 ($\Delta\omega = 25.0$) respectively. NH_3 symmetric deformation for ABPEO11, ABPEO12 and ABPEO13 were detected at 1377 ($\Delta\omega = 1.0$) 1402 ($\Delta\omega = 26.0$) and 1402 ($\Delta\omega = 25.0$) respectively. BH_3 asymmetric and symmetric deformation for pristine AB was detected at 1159 and 1064 cm^{-1} respectively. Asymmetric and symmetric BH_3 deformation for ABPEO11 was observed at 1162 ($\Delta\omega = 3.0$) and 1064 ($\Delta\omega = 0.0$) respectively. Similarly, BH_3 deformation for ABPEO12 is at 1168 ($\Delta\omega = 9.0$) and 1094 ($\Delta\omega = 30.0$) for asymmetric and symmetric deformation respectively ABPEO13 was observed at 1168 ($\Delta\omega = 9.0$) and 1096 ($\Delta\omega = 32.0$) for asymmetric and symmetric deformation respectively. The vibration mode for BH_3 is in close agreement with Petit et al. (1155 and 1053 cm^{-1} asymmetric and symmetric respectively) [58]. Xei et al. found BH_3 deformation at 1216 $cm^{-1.}$ [60] Komova et al. observed BH_3 symmetric and asymmetric deformation at 1055 and 1155 cm^{-1} respectively [62]. The peaks at 782 and 797 cm^{-1} were assigned for ^{11}BN stretching and ^{10}BN stretching. Kharel et al. observed the similar peaks at 797 and 783 cm^{-1} for pristine AB. For the polymeric composites, ABPEO11, BN stretching was detected at 782 and 797 cm^{-1} for ^{11}B and ^{10}B respectively. Unlike ABPEO11, the BN stretching in ABPEO12 was broad and only one peak was observed at 803 cm^{-1}. For ABPEO13, BN stretching peak was not that distinct. BN bending mode for AB and ABPEO11 was observed at 726 cm^{-1} however for ABPEO12 and ABPEO13 it moved more toward lower wavenumber at 619 cm^{-1}. With the increase of polymeric content in the composite sample, blue shift or hypsochromic effect is observed in NH_3 symmetric and asymmetric mode, BH_3 symmetric mode. The effect is more pronounced for composite sample with higher amount of PEO as seen in ABPEO12 and ABPEO13. In contrast, red shift or bathochromic effect was observed for BN bending mode. All these differences could be due to the interaction between the polymer and AB.

Fig. 6a displays the IR spectrum of isothermally decomposed AB and different ABPEO bulk composites at 85 °C in NH stretching region for 1 h. Similarly, Fig. 6b and c shows the IR spectrum of isothermally

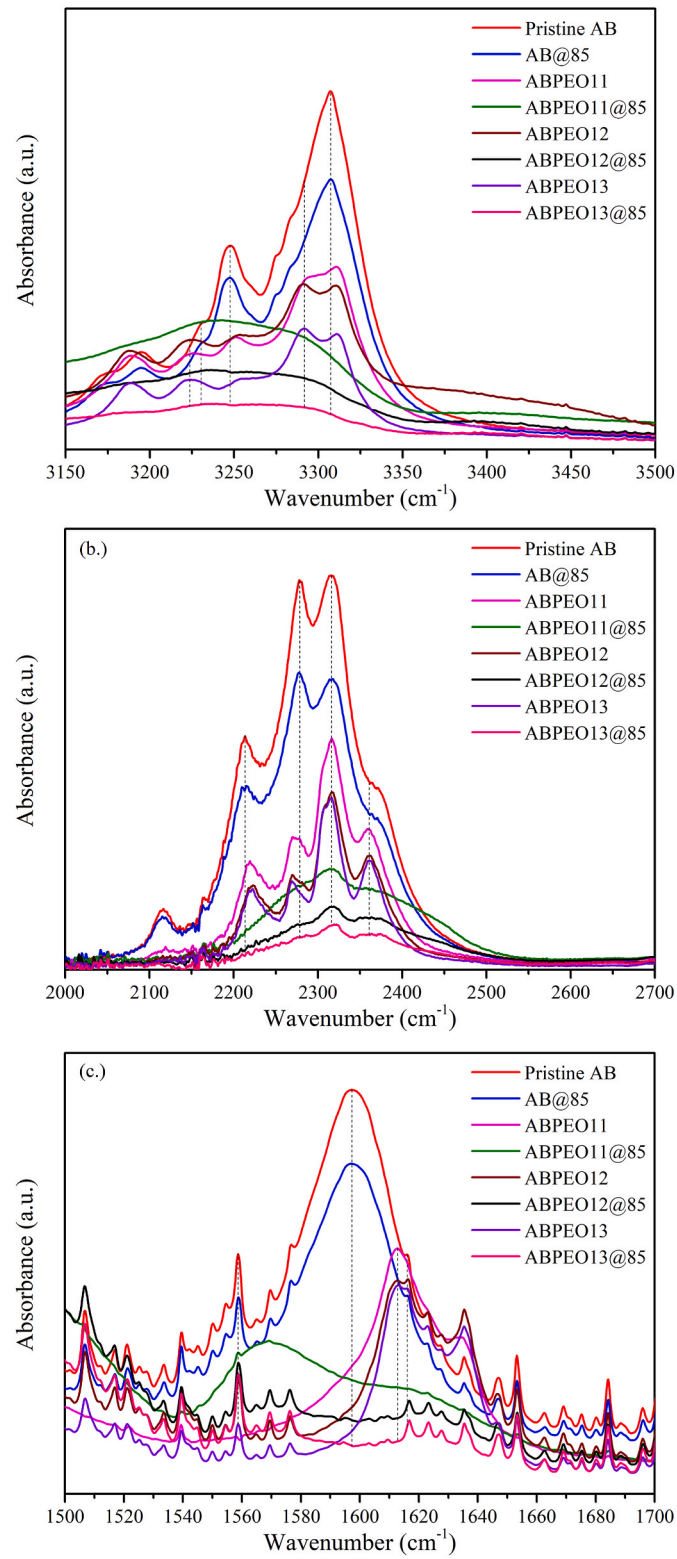

Fig. 6. Absorbance spectra (a. NH stretching, b. BH stretching and c. NH_3 deformation) of AB and its composites at room temperature and 85 °C.

decomposed AB and ABPEO composites in BH stretching and NH_3 deformation region for the same time. Table 2 displays the different vibrational mode for AB at room temperature and simulated spectrum using Spartan. Similarly, the table also present the different vibration modes for different polymeric composites. There is not much difference in different vibration modes of pristine AB at room temperature and at

Table 2
Theoretical and experimental vibration frequency for AB in pure and polymeric bulk composite form.

Modes of vibration	Comp.	Current study						Reference
		AB	ABPEO11	ABPEO12		ABPEO13		AB
N–H (a)	3722	3318	3316	3313	3294	3312	3294	3315 [61]
N–H (s)	3606	3250	3250	3255		3254		3248 [61]
B–H (a)	2608	2325	2364	2365		2269		2361 [61]
								2318 [62]
B–H (s)	2555	2280	2279	2222		2222		2324 [61]
NH_3 a.def	1855	1601	1612	1613	1636	1614	1634	1602 [61]
NH_3 s.def	1465	1376	1376	1402		1402		1375 [61]
BH_3 (a.def)	1293	1162	1167	1168		1168		1156 [61]
BH_3 (s.def)	1273	1064	1065	1080		1080		
N–B (stretch)		782	782	781		781		781 [64]
N–B (bend)	643	727	726	741		744		

*Units for peak position are in cm^{-1} s (symmetric stretching), a (asymmetric stretching), a.def (asymmetric deformation), H.int (Heteropolar interaction), s.def (symmetric deformation).

85 °C. However, for the polymeric composites, we observed the broadening of the peak at NH and BH stretching region. In NH_3 deformation region, there is no shift in the vibration frequency for AB before and after 1hrs. decomposition. Unlike AB, we see a significant change in vibration frequency for the polymeric composites of AB even at room temperature probably due to the interaction with ethereal oxygen and H-bonding. For pristine AB, in NH stretching region, the symmetric and asymmetric vibration was observed at 3247 and 3307 cm^{-1} respectively. However, for the polymeric composites, the peak in NH symmetric stretching region was observed at 3251 cm^{-1} for ABPEO11 and ABPEO12. Similarly, it was observed at 3253 cm^{-1} for ABPEO13. NH asymmetric and NH stretching modes were observed at ~3310 cm^{-1} for all polymeric composites. The most significant difference in this region was the splitting of peak for NH asymmetric mode in polymeric composites at room temperature. The decomposed polymeric sample at 85 °C has single broad peak centered ~3250 cm^{-1}. ^{11}BH asymmetric region for AB and its polymeric composites were observed at ~2316 cm^{-1}. With the increase in the polymer content, the peak at 2372 cm^{-1} assigned as ^{10}BH asymmetric stretching became more intense. For the symmetric ^{10}BH stretching, the shift was observed from 2277 cm^{-1} for AB to ~2270 cm^{-1} for bulk ABPEO composites. Unlike NH stretching, BH stretching was observed as two peaks centered at 2315 and 2365 cm^{-1} for the polymeric composites. NH_3 deformation mode is significantly affected by the addition of polymer in AB. For pristine AB, NH_3 deformation was observed at 1597 cm^{-1}. However, for the polymeric composites, it was observed around 1612 cm^{-1}. The splitting of peak in this region was rarely detected. Upon decomposition, the peak was broader. Temperature dependence of different vibration modes will be discussed in variable temperature infrared spectroscopic study of AB and its polymeric composites elsewhere [63].

3.3.2. NMR studies

3.3.2.1. ^{15}N NMR study of AB and its polymeric composites. The ^{15}N CP/MAS-NMR spectra for Pristine AB, ABPEO11, cat.ABPEO11, ABPEO12, and ABPEO13 are shown in Fig. 7. Pristine AB (Fig. 8a.) has a single peak centered at a chemical shift (δ) = 16.4 ppm confirming the presence of tertiary nitrogen atom. ^{15}N is a spin (I) = $\frac{1}{2}$ nuclei with low sensitivity due to its low abundance and low gyromagnetic ratio, $\frac{\gamma 15_N}{\gamma 1_H} = 0.10$. Upon mixing AB in a polymer matrix at 1:1 ratio (i.e. ABPEO11), the tertiary nitrogen peak at 16.4 ppm remained, although it shifts upfield slightly due to the increased electron density around the nitrogen atom when interacted with the ethereal oxygen present in PEO. However, two additional peaks at 11.7 and 8.9 ppm were observed likely due to the presence of different AB species when interacting with the PEO matrix. As hypothesized in Fig. 8, the peak at 16.4 ppm arises from the tertiary nitrogen of the dihydrogen bonded AB in the pristine AB, and the peak at 11.7 ppm might come from the relatively mobile phase of AB whose

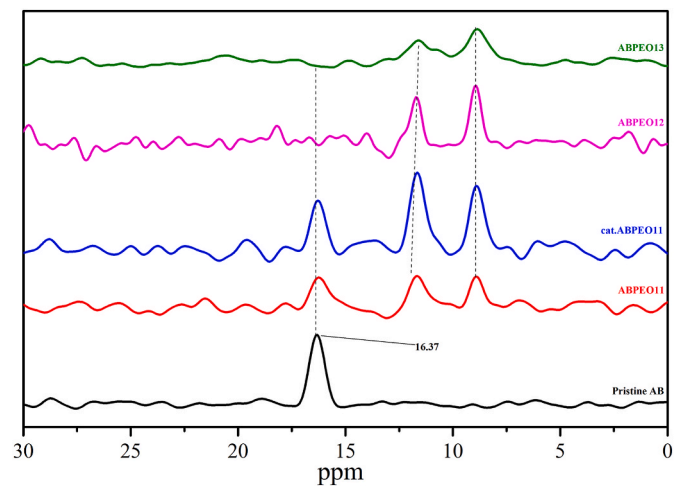

Fig. 7. ^{15}N CP/MAS-NMR spectra for Pristine AB and ABPEO composites at 25 °C.

upfield shift as compared with the chemical shift in the pristine AB is caused by increased electron density around nitrogen which might be due to the electronegativity difference (N = 3.04, H = 2.20 and B = 2.04). While the third peak for ^{15}N at 8.9 ppm might be from the nitrogen whose bonded protons are forming hydrogen bonds with the oxygen in PEO, as diagramed in Fig. 8c. Because ethereal oxygen is a good electron donor, the electron density around nitrogen is increased further, resulting in a large upfield shift. These observation confirms the change in the nitrogen environment upon the addition of polymer matrix. Upon increasing the amount of polymer content in AB, as in ABPEO12 and ABPEO13, the peak at 16.4 ppm completely disappeared, but those resonances at 11.6 and 8.9 ppm that are associated with the interaction between AB and PEO remain. H-bonding between the oxygen atom of PEO and proton from AB is the main cause of this change which has been discussed in the literature [29,65,66]. The dihydrogen bonding network of AB is affected by this H-bonding. The lone pair of electron from the oxygen of PEO may be increasing the electron density of nitrogen in ammonium moiety similar to established fiber composites of AB and PEO [29]. In this study in the polymeric composites with mass ratio 1:2 and 1:3, the tertiary N shift disappears which strongly support the interaction of AB/PEO and the disturbed dihydrogen bonding network of AB.

3.3.2.2. ^{11}B NMR study of AB and its polymeric composites heated in situ at 85 °C. The NMR spectrum for pristine AB and its polymeric composites were recorded at room temperature before increasing the

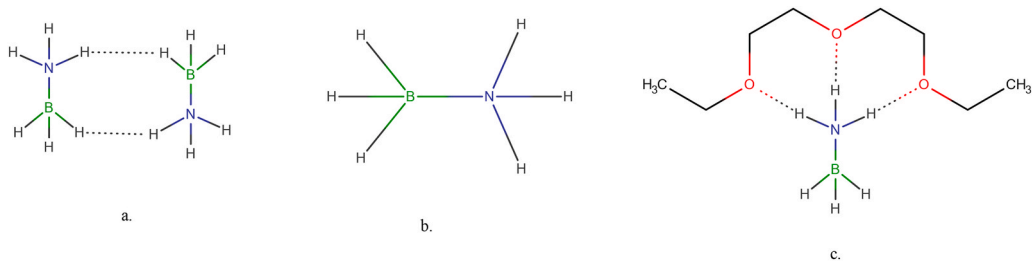

Fig. 8. (a.) AB without any interaction showing dihydrogen bonding (b.) mobile phase of AB and (c.) Possible interaction of AB with ethereal oxygen present in PEO.

temperature to 85 °C. Once the temperature reached 85 °C, the spectrum was recorded every half hour. All of the gaseous products evolved during the thermolytic dissociation of AB and its polymeric composites were evaporated so the peaks associated with a gaseous product like H_2, NH_3 were not observed. Fig. 9 displays the major peaks associated with AB and AB byproducts upon decomposition. At room temperature, ^{11}B spectrum shows the typical second-order quadrupolar broadened lineshape with singularities appearing at 26.6 and −25.2 ppm, which is contributed to the BH_3 moiety of AB. Once AB started to decompose at 85 °C, this lineshape remained but additional peaks started to show up. The peak at −39.2 ppm is assigned to diammoniate of diborane (DADB) which is the reaction intermediate before releasing hydrogen. In addition to that, we observed the peak at −23.9 ppm which is due to the BH_3 moiety in mobile phase of AB [18]. The relatively lesser intense peak was observed at −22.9 ppm assigned for BH_3 end group. Similarly, the peak at −14.6, −13.6 and, −12.3 ppm is from BH_2 of DADB, BH_2 linear dimer and BH group respectively [18].

Fig. 10 shows the ^{11}B spectra for the pristine AB, ABPEO11, and ABPEO12 at 25 °C Clearly, the lineshapes for ABPEO11 and ABPEO12 become complex as compared with that for the pristine AB, implying the presence of different BH_3 moieties of AB when composited with the PEO matrix, thus confirming the interaction of AB with PEO. It is reasonable to assume, based on the ^{11}B lineshape for the pristine AB, that the central transition lineshape for each BH_3 moiety has two singularities. Therefore, it is expected to have a total of six and four singularities for ABPEO11 and ABPEO12, respectively, based on their ^{15}N spectra (c.f. Fig. 7).

Figs. 11–13 display ^{11}B MAS NMR spectra at 85 °C for over 6 h for the pristine AB, ABPEO11, and ABPEO12 respectively. As shown in Fig. 11, when holding the pristine AB at 85 °C for up to 0.5 h, no change could be observed in the spectra. However, when incubating at 85 °C for 1.0 h,

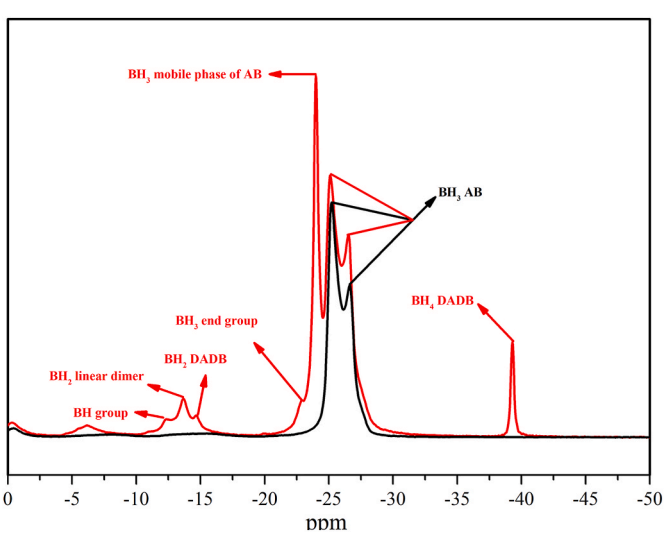

Fig. 9. ^{11}B MAS NMR of pure AB at room temperature and 85 °C with major peak assignments.

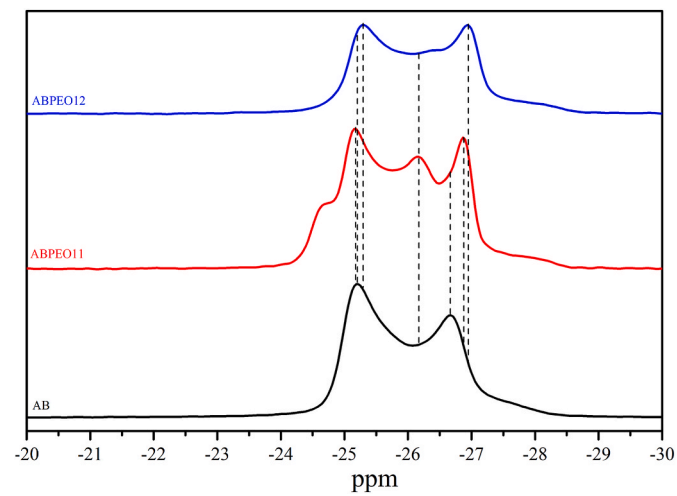

Fig. 10. ^{11}B MAS-NMR spectra for Pristine AB, ABPEO11, and ABPEO12 at 25 °C.

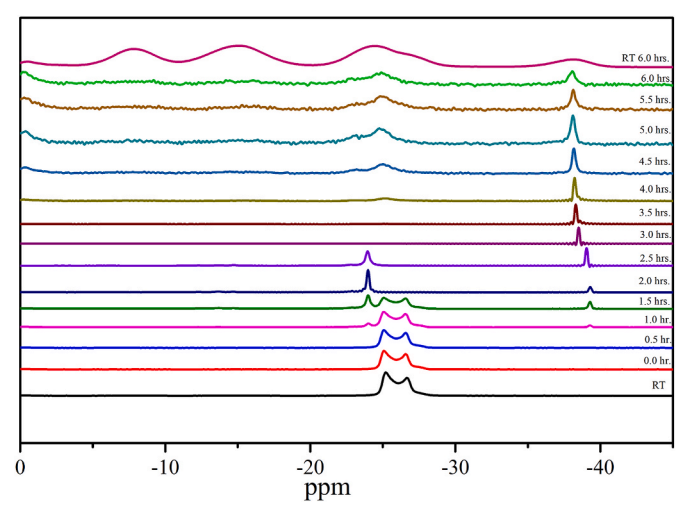

Fig. 11a. ^{11}B MAS-NMR spectra for Pristine AB at 85 °C for 6 h.

new peaks at $\delta_{AB} = -24\,ppm$ and $\delta_{AB} = -39\,ppm$ start to appear and gain in intensities with a longer incubation time. The former one can be assigned as mobile phase of AB (AB*) and the later as BH_4 in diammoniate of diborane (DADB) [29]. The upfield movement of DADB peak indicated the decreased symmetry for boron which might present in the vicinity of boron atom of polyamidoborane (PAB) moieties [67]. This supports the hypothesis proposed by Shaw et al. for the nucleation and growth of the PAB chain by the addition of new AB molecule [68]. AB after the decomposition for 1.5 h three different peaks were observed at $\delta_{AB} = -14.66, -13.67$ *and* $-$ 12.31 ppm in Fig. 11b assigned for BH_2

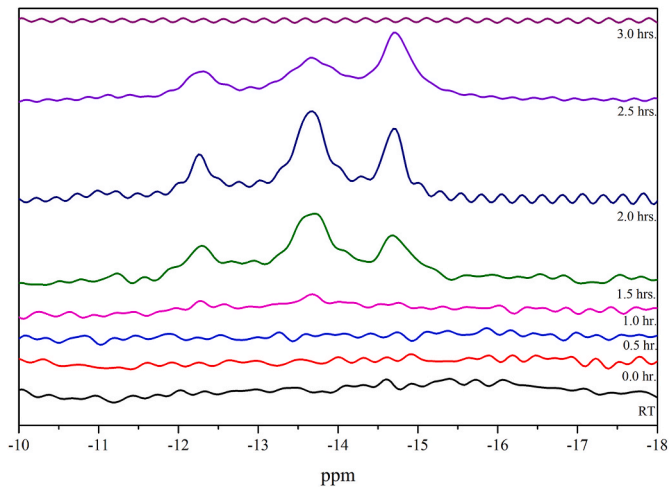

Fig. 11b. The corresponding spectra with vertically enlarged scale in the region of −10 and −18 ppm.

of DADB, BH_2 of linear dimer and BH group respectively as also seen in Fig. 9 with a zoomed scale. After the decomposition for 2 h the peak associated with BH_3 of AB completely disappeared. Only the peaks associated with DADB and AB* were observed. However, there is no significant change for the polymeric composites. After the incubation time of 3 h, the peak assigned for DADB moved slightly upfield to −38.46 ppm. After 4.5 h, a new peak starts to appear at $\delta_{AB} = -7.5$ ppm assigned for BH. The three different peaks about the proximity of $\delta_{AB} = -14$ ppm merge to form a single peak at $\delta_{AB} = -14.9$ ppm. The peak for AB and AB* are less intense by the end of 4 h but became more intense at 4.5 h. The spectrum was stable after 4.5 h. There were no new peaks formed. However, upon cooling back to room temperature after 6 h, the peaks for DADB, BH_3 BH_2 (DADB, linear dimer) BH became broad.

Unlike the pristine AB that starts to decompose after 1 h incubation time at 85 °C as indicated by the presence of DADB and AB*, ABPEO11 and ABPEO12 got readily decomposed at 85 °C as indicated by the presence of BH_4 ($\delta_{ABPEO11} = -39.1$ *and* $\delta_{ABPEO12} = -39.2$) due to the formation of DADB and presence of AB* [68,69]referred as the mobile phase of AB with the $\delta_{ABPEO11} = -23.28$ *and* $\delta_{ABPEO12} = -23.34$ *ppm* in both ABPEO11 and ABPEO12. After 1 h of incubation at 85 °C. a broad peak at $\delta_{ABPEO11} = -14.21$ was assigned for BH_2 in Figs. 12 and 13 respectively. BO interaction was also observed at around 0.29 ppm for ABPEO11 and ~0.12 ppm for ABPEO12 as observed by Nathanson et al.

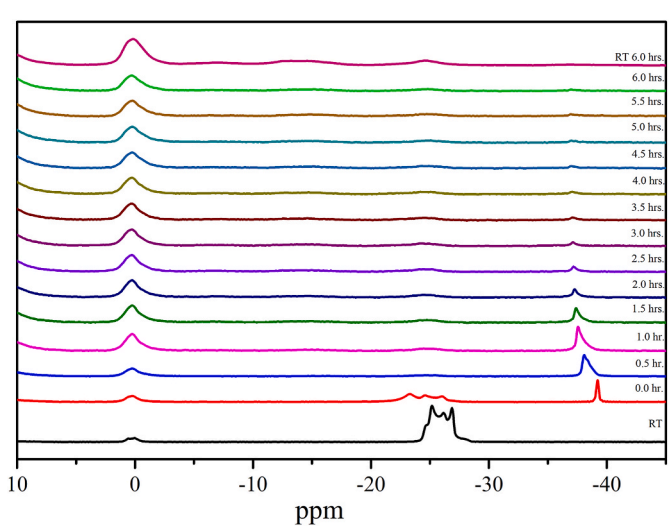

Fig. 12. ^{11}B MAS-NMR spectra for ABPEO11 at 85 °C for 6 h.

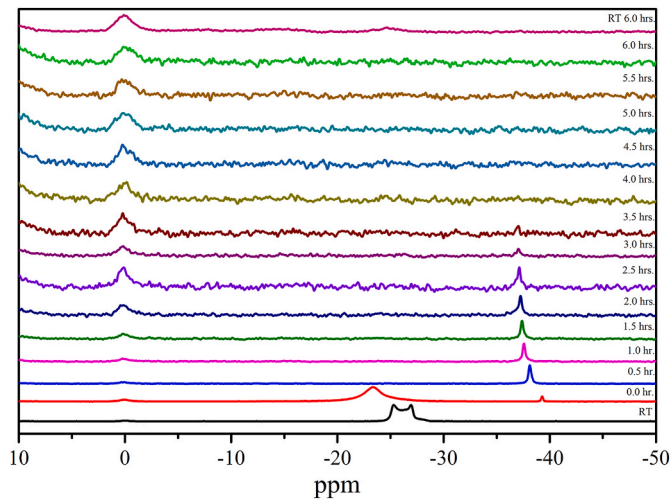

Fig. 13. ^{11}B MAS-NMR spectra for ABPEO12 at 85 °C for 6 h.

[29]. There is also a shift for DADB from ~ −39 ppm moving upfield to ~ −38 ppm for both ABPEO11 and ABPEO12. The further decomposition of ABPEO11 and ABPEO12 were characterized by the lowering in the intensity of AB*, increased intensity of BO and upfield movement of DADB.

The polymeric composites of AB showed improved decomposition and favored the path for the early formation of PAB which might have lowered the decomposition temperature for the polymeric composites of AB.

4. Conclusion

The primary objective of the study was to have a comparative investigation on the dehydrogenation properties of AB and its polymeric composites with and without using $MgCl_2$ as a catalyst. We used thermal, IR, room temperature ^{15}N MAS-NMR, room temperature and isothermal ^{11}B MAS-NMR techniques to understand the interaction of AB with PEO. The high-temperature decomposition study of AB and its composites revealed the decrease in the decomposition temperature when AB is mixed in the polymer matrix. For pristine AB and ABPEO composites at ramp 5 °C/min, the first dehydrogenation temperature ranged from 117 °C for pristine AB to 85 °C for cat.ABPEO12. Unlike pristine AB and its bulk polymeric composites, the polymeric composites with 5 % $MgCl_2$ catalyst showed early decomposition. We also observed a decrease in the activation energy of the polymeric composites when compared with pristine AB. Though we observed early decomposition of catalytic composites, the activation energy is relatively higher when compared with the one without the catalyst of same mass ratio. Unlike catalytic composites, polymeric composites have relatively lower activation energy. The activation energy for AB was calculated to be 149 kJ/mol. However, for ABPEO11, the activation energy was calculated to be 108 kJ/mol according to Kissinger method. The kinetics of AB was improved when it was dispersed in polymer matrix.

IR study was performed to understand the chemical interaction of AB with PEO. ATR study was performed to identify different vibration frequency for AB and PEO. At room temperature, NH_3 stretching frequency for AB and ABPEO11 is close to each other, but there is a significant difference in the vibration frequency with the higher mass ratio. Room temperature IR study revealed that NH_3 moiety in ABPEO composites were significantly affected. The splitting of peaks in NH stretching and NH_3 deformation region was observed at room temperature. It may be due to the formation of H-bonding between the ethereal oxygen and hydrogen atom from NH_3 moiety. Also, from the decomposition IR study, pristine AB took longer time for decomposition at 85 °C. Unlike AB, the polymeric composites readily started to decompose.

^{15}N and ^{11}B high-resolution MAS-NMR techniques were conducted to understand the possible interaction, bonding, and dehydrogenation mechanism. ^{15}N NMR enabled us to observe the change in the nitrogen environment. The presence of a single peak in pristine AB confirms only one type of nitrogen. However, upon the addition of polymer, three different peaks were observed which may be due to the breaking of dihydrogen bonding network of AB and forming hydrogen bonding with the ethereal oxygen of PEO. The three-hydrogen atom in AB might interact in two different ways either by dative H-bonding between the molecule or H-bonding with the ethereal oxygen giving rise to different peaks for the polymeric composites in ^{15}N NMR. For the polymeric composites with higher mass ratio, ABPEO12 and ABPEO13, the peak from NH_3 moiety of pristine AB is lost, which may be due to the interaction of all AB molecule within the polymer. Mixing AB with PEO is expected to produce a new crystalline phase. These changes in AB with the addition of polymer was caused by the electron dense ethereal oxygen (-O) in PEO backbone. ^{11}B NMR study also supports the possible interaction of AB with PEO molecule. At room temperature, two peaks for BH_3 from AB was observed at −25.18 ppm and −26.67 ppm. However, for ABPEO11 composites, two additional peaks were observed at −24.64 ppm and −26.16 ppm. The appearance of these two peaks other than the peak form BH_3 of moiety is another proof of possible interaction with PEO. Upon increasing the polymer content, one of the additional peak for the mobile phase of AB at −24.64 ppm was lost. From the decomposition IR study and isothermal ^{11}B NMR study, we concluded the longer incubation time is needed for pristine AB, however, PEO composites decompose readily at 85 °C.

In summary, we investigated the thermal and vibrational properties of AB and its ABPEO bulk composites. Mixing AB in the polymer matrix improved the thermal and kinetic properties of AB. The hydrogen release temperature is lower when compared with pristine AB. The NMR study revealed the change in the nitrogen and boron environment when AB is confined in PEO matrix. This change may be due to the interaction of more electronegative ethereal oxygen with nitrogen. ABPEO composites decompose earlier without incubation time which makes them one of the alternative for the solid-state hydrogen storage medium.

CRediT authorship contribution statement

Krishna Kharel: Writing – review & editing, Writing – original draft, Formal analysis, Data curation. **Riqiang Fu:** Writing – review & editing, Resources, Methodology, Investigation, Funding acquisition, Formal analysis, Data curation. **Emily Ingram:** Writing – review & editing, Investigation, Formal analysis, Data curation. **Caitlyn Clark:** Formal analysis, Data curation. **Özge Günaydın:** Writing – review & editing, Writing – original draft, Visualization, Validation, Supervision, Software, Resources, Project administration, Methodology, Investigation, Funding acquisition, Formal analysis, Data curation, Conceptualization.

Declaration of competing interest

The authors declare that they have no known competing financial interests or personal relationships that could have appeared to influence the work reported in this paper.

Data availability

Data will be made available on request.

Acknowledgments

This research was supported by Welch Foundation (V-0004). All NMR experiments were carried out at the National High Magnetic Field Laboratory (NHMFL) supported by the NSF Cooperative agreement no. DMR-1644779 and DMR-2128556 and the State of Florida.

References

[1] M. Navlani-García, K. Mori, Y. Kuwahara, H. Yamashita, Recent strategies targeting efficient hydrogen production from chemical hydrogen storage materials over carbon-supported catalysts, NPG Asia Mater. 10 (2018) 277–292.
[2] A. Klerke, C.H. Christensen, J.K. Nørskov, T. Vegge, Ammonia for hydrogen storage: challenges and opportunities, J. Mater. Chem. 18 (2008) 2304–2310.
[3] M. Aziz, A.T. Wijayanta, A.B.D. Nandiyanto, Ammonia as effective hydrogen storage: a review on production, storage and utilization, Energies 13 (2020) 3062–3086.
[4] D. Wechsler, Y. Cui, D. Dean, B. Davis, P.G. Jessop, Production of H2 from combined endothermic and exothermic hydrogen carriers, J. Am. Chem. Soc. 130 (2008) 17195–17203.
[5] B. Loges, A. Boddien, F. Gärtner, H. Junge, M. Beller, Catalytic generation of hydrogen from formic acid and its derivatives: useful hydrogen storage materials, Top. Catal. 53 (2010) 902–914.
[6] F. Frusteri, G. Bonura, 5 - hydrogen production by reforming of bio-alcohols, in: V. Subramani, A. Basile, T.N. Veziroğlu (Eds.), Compendium of Hydrogen Energy, Woodhead Publishing, Oxford, 2015, pp. 109–136.
[7] S. Saxena, S. Kumar, V. Drozd, Int. J. Hydrogen Energy 36 (2011) 4366–4369.
[8] T. Kobayashi, H. Takahashi, Novel CO2 electrochemical reduction to methanol for H2 storage, Energy Fuels 18 (2004) 285–286.
[9] P. Preuster, C. Papp, P. Wasserscheid, Liquid organic hydrogen carriers (LOHCs): toward a hydrogen-free hydrogen economy, Acc. Chem. Res. 50 (2017) 74–85.
[10] X.-B. Zhang, S. Han, J.-M. Yan, M. Chandra, H. Shioyama, K. Yasuda, N. Kuriyama, T. Kobayashi, Q. Xu, A new fuel cell using aqueous ammonia-borane as the fuel, J. Power Sources 168 (2007) 167–171.
[11] M. Diwan, D. Hanna, A. Varma, Method to release hydrogen from ammonia borane for portable fuel cell applications, Int. J. Hydrogen Energy 35 (2010) 577–584.
[12] E. Pawelczyk, N. Łukasik, I. Wysocka, A. Rogala, J. Gębicki, Recent progress on hydrogen storage and production using chemical hydrogen carriers, Energies 15 (2022) 4964–4997.
[13] M. Liu, L. Zhou, X. Luo, C. Wan, L. Xu, Recent advances in noble metal catalysts for hydrogen production from ammonia borane, Catalysts 10 (2020) 788–822.
[14] J. Zhang, J.W. Lee, Progress and prospects in thermolytic dehydrogenation of ammonia borane for mobile applications, Kor. J. Chem. Eng. 29 (2012) 421–431.
[15] X. Yang, D.A. Bulushev, J. Yang, Q. Zhang, New liquid chemical hydrogen storage technology, Energies 15 (2022) 6360–6377.
[16] K. Kharel, R. Gangineni, L. Ware, Y. Lu, E.K. Wujcik, S.Y. Wei, O. Gunaydin-Sen, Dehydrogenation properties of ammonia borane-polyacrylamide nanofiber hydrogen storage composites, J. Mater. Sci. 52 (2017) 4894–4902.
[17] W.W. Zhan, Q.L. Zhu, Q. Xu, Dehydrogenation of ammonia borane by metal nanoparticle catalysts, ACS Catal. 6 (2016) 6892–6905.
[18] A.R. Ploszajski, M. Billing, A.S. Nathanson, M. Vickers, S.M. Bennington, Freeze-dried ammonia borane-polyethylene oxide composites: phase behaviour and hydrogen release, Int. J. Hydrogen Energy 43 (2018) 5645–5656.
[19] M. Navlani-García, D. Salinas-Torres, D. Cazorla-Amorós, Hydrolytic dehydrogenation of ammonia borane attained by Ru-based catalysts: an auspicious option to produce hydrogen from a solid hydrogen carrier molecule, Energies 14 (2021) 2199–2218.
[20] X. Chen, J.-C. Zhao, S.G. Shore, The roles of dihydrogen bonds in amine borane chemistry, Acc. Chem. Res. 46 (2013) 2666–2675.
[21] A. Rossin, M. Peruzzini, Ammonia–borane and amine–borane dehydrogenation mediated by complex metal hydrides, Chem. Rev. 116 (2016) 8848–8872.
[22] M.G. Hu, R.A. Geanangel, W.W. Wendlandt, The thermal decomposition of ammonia borane, Thermochim. Acta 23 (1978) 249–255.
[23] V. Sit, R.A. Geanangel, W.W. Wendlandt, The thermal dissociation of NH3BH3, Thermochim. Acta 113 (1987) 379–382.
[24] T. Hugle, M.F. Kuhnel, D. Lentz, Hydrazine borane: a promising hydrogen storage material, J. Am. Chem. Soc. 131 (2009) 7444–7446.
[25] M. Valero-Pedraza, D. Cot, E. Petit, K.F. Aguey-Zinsou, J.G. Alauzun, U.B. Demirci, Ammonia borane nanospheres for hydrogen storage, ACS Appl. Nano Mater. 2 (2019) 1129–1138.
[26] Mei-Jing Fang, Yu-Chang Lin, Jen-Yu Jan, Ting-Hsuan Lai, Ping-Yen Hsieh, Ming-Yu Kuo, Yi-Hsuan Chiu, Chun-Wen Tsao, Yi-An Chen, Yu-Ting Wang, Yi-Jia Hong, Jhen-Yang Wu, Yew Chung Sermon Wu, Yan-Gu Lin, Tso-Fu Mark Chang, Chun-Yi Chen, Masato Sone, Sue-Min Chang, Chung-Liang Chang, Yung-Jung Hsu, Au@Cu2o Core@Shell nanocrystals as sustainable catalysts for efficient hydrogen production from ammonia borane, Appl. Catal. B Environ. 324 (2023) 122198–122211.
[27] S.F. Li, Z.W. Tang, Y.B. Tan, X.B. Yu, Polyacrylamide blending with ammonia borane: a polymer supported hydrogen storage composite, J. Phys. Chem. C 116 (2012) 1544–1549.
[28] J. Zhao, J. Shi, X. Zhang, F. Cheng, J. Liang, Z. Tao, J. Chen, A soft hydrogen storage material: poly(methyl acrylate)-confined ammonia borane with controllable dehydrogenation, Adv. Mater. 22 (2010) 394–397.
[29] A.S. Nathanson, A.R. Ploszajski, M. Billing, J.P. Cook, D.W.K. Jenkins, T.F. Headen, Z. Kurban, A. Lovell, S.M. Bennington, Ammonia borane–polyethylene oxide composite materials for solid hydrogen storage, J. Mater. Chem. A 3 (2015) 3683–3691.
[30] R. Seemaladinne, S. Pati, K. Kharel, A. Bafana, A. al-Wahish, E.K. Wujcik, O. Gunaydin-Sen, Ammonia borane with polyvinylpyrrolidone as a hydrogen storage material: comparison of different molecular weights, J. Phys. Chem. Solid. 110 (2017) 394–400.

[31] O. Metin, S. Ozkar, Hydrogen generation from the hydrolysis of ammonia-borane and sodium borohydride using water-soluble polymer-stabilized cobalt(0) nanoclusters catalyst, Energy Fuels 23 (2009) 3517–3526.
[32] H. Erdoğan, Ö. Metin, S. Özkar, In situ-generated PVP-stabilized palladium(0) nanocluster catalyst in hydrogen generation from the methanolysis of ammonia–borane, Phys. Chem. Chem. Phys. 11 (2009) 10519–10525.
[33] D. Ke, Y. Li, J. Wang, L. Zhang, J. Wang, X. Zhao, S. Yang, S. Han, Facile fabrication of poly(amidoamine) (PAMAM) dendrimers-encapsulated Ag–Co bimetallic nanoparticles for highly efficient dehydrogenation of ammonia borane, Int. J. Hydrogen Energy 41 (2016) 2564–2574.
[34] J. Alipour, A.M. Shoushtari, A. Kaflou, Ammonia borane confined by poly(methyl methacrylate)/multiwall carbon nanotube nanofiber composite, as a polymeric hydrogen storage material, J. Mater. Sci. 50 (2015) 3110–3117.
[35] Z. Li, G. Zhu, G. Lu, S. Qiu, X. Yao, Ammonia borane confined by a Metal−Organic framework for chemical hydrogen storage: enhancing kinetics and eliminating ammonia, J. Am. Chem. Soc. 132 (2010) 1490–1491.
[36] G. Moussa, S. Bernard, U.B. Demirci, R. Chiriac, P. Miele, Room-temperature hydrogen release from activated carbon-confined ammonia borane, Int. J. Hydrogen Energy 37 (2012) 13437–13445.
[37] J. Richard, S.L. Cid, J. Rouquette, A. van der Lee, S. Bernard, J. Haines, Pressure-induced insertion of ammonia borane in the siliceous zeolite, silicalite-1F, J. Phys. Chem. C 120 (2016) 9334–9340.
[38] L.J. Zhang, G.L. Xia, Y. Ge, C.Y. Wang, Z.P. Guo, X.G. Li, X.B. Yu, Ammonia borane confined by nitrogen-containing carbon nanotubes: enhanced dehydrogenation properties originating from synergetic catalysis and nanoconfinement, J. Mater. Chem. A 3 (2015) 20494–20499.
[39] Z. Lu, B.L. Conley, T.J. Williams, A three-stage mechanistic model for ammonia–borane dehydrogenation by shvo's catalyst, Organometallics 31 (2012) 6705–6714.
[40] A. Staubitz, M.E. Sloan, A.P.M. Robertson, A. Friedrich, S. Schneider, P.J. Gates, J. S.a.d. Günne, I. Manners, Catalytic dehydrocoupling/dehydrogenation of N-Methylamine-Borane and ammonia-borane: synthesis and characterization of high molecular weight polyaminoboranes, J. Am. Chem. Soc. 132 (2010) 13332–13345.
[41] Ö. Metin, S. Duman, M. Dinç, S. Özkar, Oleylamine-Stabilized palladium(0) nanoclusters as highly active heterogeneous catalyst for the dehydrogenation of ammonia borane, J. Phys. Chem. C 115 (2011) 10736–10743.
[42] S.F. Li, Y.H. Guo, W.W. Sun, D.L. Sun, X.B. Yu, Platinum nanoparticle functionalized CNTs as nanoscaffolds and catalysts to enhance the dehydrogenation of ammonia-borane, J. Phys. Chem. C 114 (2010) 21885–21890.
[43] P. Chandrasekaran, A.F. Greene, K. Lillich, S. Capone, J.T. Mague, S. DeBeer, J. P. Donahue, A structural and spectroscopic investigation of octahedral platinum bis (dithiolene)phosphine complexes: platinum dithiolene internal redox chemistry induced by phosphine association, Inorg. Chem. 53 (2014) 9192–9205.
[44] F. Cheng, H. Ma, Y. Li, J. Chen, Ni1-xPtx (x = 0−0.12) hollow spheres as catalysts for hydrogen generation from ammonia borane, Inorg. Chem. 46 (2007) 788–794.
[45] W.Q. Feng, L. Yang, N. Cao, C. Du, H.M. Dai, W. Luo, G.Z. Cheng, In situ facile synthesis of bimetallic CoNi catalyst supported on graphene for hydrolytic dehydrogenation of amine borane, Int. J. Hydrogen Energy 39 (2014) 3371–3380.
[46] A.J. Amali, K. Aranishi, T. Uchida, Q. Xu, PdPt nanocubes: a high-performance catalyst for hydrolytic dehydrogenation of ammonia borane, Part. Part. Syst. Char. 30 (2013) 888–892.
[47] T. Kamegawa, T. Nakaue, Complete hydrogen release from aqueous ammonia-borane over a platinum-loaded titanium dioxide photocatalyst, Chem. Commun. 51 (2015) 16802–16805.
[48] M.E. Bluhm, M.G. Bradley, R. Butterick, U. Kusari, L.G. Sneddon, Amineborane-based chemical hydrogen storage: enhanced ammonia borane dehydrogenation in ionic liquids, J. Am. Chem. Soc. 128 (2006) 7748–7749.
[49] J.-Y. Chung, C.-W. Liao, Y.-W. Chang, B.K. Chang, H. Wang, J. Li, C.-Y. Wang, Influence of metal–organic framework porosity on hydrogen generation from nanoconfined ammonia borane, J. Phys. Chem. C 121 (2017) 27369–27378.
[50] R.Q. Zhong, R.Q. Zou, T. Nakagawa, M. Janicke, T.A. Semelsberger, A.K. Burrell, R. E. Del Sesto, Improved hydrogen release from ammonia-borane with ZIF-8, Inorg. Chem. 51 (2012) 2728–2730.
[51] H. Yang, Z. Li, K. Liu, F. Meng, C. Niu, Clean hydrogen release from ammonia borane in a metal–organic framework with unsaturated coordinated Tm3+, J. Phys. Chem. C 119 (2015) 2260–2265.
[52] H. Li, Y. Yan, S. Feng, Y. Chen, L. Li, L. Zhang, Z. Yang, Hydrogen release mechanism and performance of ammonia borane catalyzed by transition metal catalysts Cu-Co/MgO(100), Int. J. Energy Res. 43 (2019) 921–930.
[53] M.J. Starink, A new method for the derivation of activation energies from experiments performed at constant heating rate, Thermochim. Acta 288 (1996) 97–104.
[54] R.M.R. Wellen, E.L. Canedo, On the Kissinger equation and the estimate of activation energies for non-isothermal cold crystallization of PET, Polym. Test. 40 (2014) 33–38.
[55] X. Ding, J. Feng, T. Xia, X. Yuan, D. Liu, Y. Li, Q. Zhang, The superior desorption properties of MgCl2-added ammonia borane compared to MgF2-added systems—the unexpected role of MgCl2 interacting with [NH3] units, RSC Adv. 7 (2017) 36684–36687.
[56] Y. Yang, H. Huo, Investigation of structures of PEO-MgCl2 based solid polymer electrolytes, J. Polym. Sci. B Polym. Phys. 51 (2013) 1162–1174.
[57] L.L. Yang, A.R. McGhie, G.C. Farrington, Ionic conductivity in complexes of poly (ethylene oxide) and MgCl2, J. Electrochem. Soc. 133 (2019) 1380–1385.
[58] J.-F. Petit, P. Miele, U.B. Demirci, Ammonia borane H3N-BH3 for solid-state chemical hydrogen storage: different samples with different thermal behaviors, Int. J. Hydrogen Energy 41 (2016) 15462–15470.
[59] J. Smith, K.S. Seshadri, D. White, Infrared spectra of matrix isolated BH3 NH3, BD3 ND3, and BH3 ND3, J. Mol. Spectrosc. 45 (1973) 327–337.
[60] S.T. Xie, Y. Song, Z.X. Liu, In situ high-pressure study of ammonia borane by Raman and IR spectroscopy, Canadian Journal of Chemistry-Revue Canadienne De Chimie 87 (2009) 1235–1247.
[61] J. Zhang, Y. Zhao, D.L. Akins, J.W. Lee, CO2-Enhanced thermolytic H2 release from ammonia borane, J. Phys. Chem. C 115 (2011) 8386–8392.
[62] O.V. Komova, N.L. Kayl, G.V. Odegova, O.V. Netskina, V.I. Simagina, Destabilization of NH3BH3 by water during hydrothermolysis as a key factor in the high hydrogen evolution rates, Int. J. Hydrogen Energy 41 (2016) 17484–17495.
[63] K. Kharel, O. Günaydın-Şen, Lamar University, 2018.
[64] G. Srinivas, J. Ford, W. Zhou, T. Yildirim, Zn-MOF assisted dehydrogenation of ammonia borane: enhanced kinetics and clean hydrogen generation, Int. J. Hydrogen Energy 37 (2012) 3633–3638.
[65] Y. Kim, H. Baek, J.H. Lee, S. Yeo, K. Kim, S.-J. Hwang, B. Eun, S.W. Nam, T.-H. Lim, C.W. Yoon, Metal-free, polyether-mediated H2-release from ammonia borane: roles of hydrogen bonding interactions in promoting dehydrogenation, Phys. Chem. Chem. Phys. 15 (2013) 19584–19594.
[66] H.M. Colquhoun, G. Jones, J.M. Maud, J.F. Stoddart, D.J. Williams, Crystal and supramolecular structures of complexes of BF3NH3 and BH3NH3 with 18-crown-6, J. Chem. Soc. Dalton Trans. (1984) 63–66.
[67] B. Kang, G. Ceder, Battery materials for ultrafast charging and discharging, Nature 458 (2009) 190.
[68] W.J. Shaw, J.C. Linehan, N.K. Szymczak, D.J. Heldebrant, C. Yonker, D. M. Camaioni, R.T. Baker, T. Autrey, In situ multinuclear NMR spectroscopic studies of the thermal decomposition of ammonia borane in solution, Angew. Chem. Int. Ed. 47 (2008) 7493–7496.
[69] A.C. Stowe, W.J. Shaw, J.C. Linehan, B. Schmid, T. Autrey, In situ solid state 11B MAS-NMR studies of the thermal decomposition of ammonia borane: mechanistic studies of the hydrogen release pathways from a solid state hydrogen storage material, Phys. Chem. Chem. Phys. 9 (2007) 1831–1836.